Bilayers of Rydberg atoms as a quantum simulator for unconventional superconductors

Bilayers of Rydberg atoms as a quantum simulator for unconventional superconductors.

J.P. Hague[1] and C. MacCormick[1]

[1] *The Open University, Walton Hall, Milton Keynes, MK7 6AA, UK*

(Dated: 12th December 2011)

In condensed matter, it is often difficult to untangle the effects of competing interactions, and this is especially problematic for superconductors. Quantum simulators may help: here we show how exploiting the properties of highly excited Rydberg states of cold fermionic atoms in a bilayer lattice can simulate electron-phonon interactions in the presence of strong correlation - a scenario found in many unconventional superconductors. We discuss the core features of the simulator, and use numerics to compare with condensed matter analogues. Finally, we illustrate how to achieve a practical, tunable implementation of the simulation using 'painted spot' potentials.

PACS numbers: 37.10.Jk, 32.80.Ee, 74.20.-z

Cold atom quantum simulators offer an important new approach to the study of correlated electron phenomena without the limitations of computational or analytical techniques. For example, cold atoms have recently been used as quantum simulators to investigate models of condensed matter such as the Hubbard model of strong local Coulomb repulsion, which is important for the understanding of cuprate superconductors [1, 2]. This has led to direct observation of important phenomena such as the superfluid to Mott insulator transition [3, 4].

Besides the cuprates, there are several superconductors with high transition temperatures, many of which have important roles for electron-phonon interactions, and repulsion driven correlated electron phenomena such as antiferromagnetism. Fulleride superconductors of the family A_3C_{60} have phonon driven transition temperatures [5] of up to 40K [6], but also exhibit antiferromagnetism at appropriate dopings and structures [7]. Superconductivity in bismuthates with $T_C > 30K$ [8] is probably due to strong couplings of localized electrons to the lattice [9] (as evidenced by a large isotope shift [10, 11]). High transition temperatures have also been achieved in the borocarbides [12, 13] ($T_C = 23$K) and chloronitrides [14] ($T_C = 25$K). The more conventional layered MgB_2 and graphite intercalation compounds are also interesting. Even the cuprate superconductors, where superconductivity is thought by many to be driven by antiferromagnetic fluctuations [15], show isotope shifts [16] and other effects such as kinks [17] that may be attributed to a non-trivial interplay between strong correlations and lattice vibrations.

Owing to the importance of electron-phonon interactions in condensed matter, reliable numerical methods have been sought, but even very simplified models [18] are extremely hard to simulate. Simulations either have to deal with the potentially infinite number of phonons associated with even a single electron, or retardation effects if the phonons are integrated out. A key problem in many advanced materials is that electrons are localized to atomic orbitals and accordingly the Fermi energy is small. This localization means that dimensionless electron-phonon couplings are relatively strong and phonon frequencies can be large at around 10% of the Fermi energy. Even moderate couplings with intermediate frequency phonons can lead to consequences that cannot be predicted with perturbation theory and other analytics. Such couplings can cause additional difficulties for numerics, that are often most efficient in the extreme limits of weak or strong coupling. Recent advances in continuous time quantum Monte Carlo (CTQMC) cluster impurity solvers for dynamical mean field theories offer a state of the art for numerical simulations of Hubbard and Holstein models (for a review see 19). Such simulations are currently limited to ~ 36 site clusters for Hubbard models and 12 site clusters for Holstein models, limiting the range of spatial fluctuations that can be simulated in 2D to a few sites.

Quantum simulation of lattice effects has proved difficult to implement. The existence of quantum simulators with a high degree of control over the form of interactions has the potential to provide significant insight into the subtle interplay between electronic correlation, lattice vibration and phenomena such as superconductivity and colossal magnetoresistance. We propose an approach for simulating fermionic Hubbard models extended to include strong long-range interactions with lattice vibrations, by discussing Rydberg states of cold atoms in bilayer lattices. Such a simulator is likely to shed light on a wide range of unconventional superconductors with transition temperatures greater than 30K, and might resolve aspects of ongoing debates on cuprate mechanisms.

A quantum simulator for complex electronic systems such as unconventional superconductors should have the following main characteristics: (1) It must be able to simulate fermions (2) It should be capable of simulating all filling factors up to and including half filling (1 fermion per lattice site) where the physics of materials with complex phase diagrams is most interesting (3) All parameters, including the phonon frequency, electron-phonon coupling, Hubbard U and hopping t should be highly

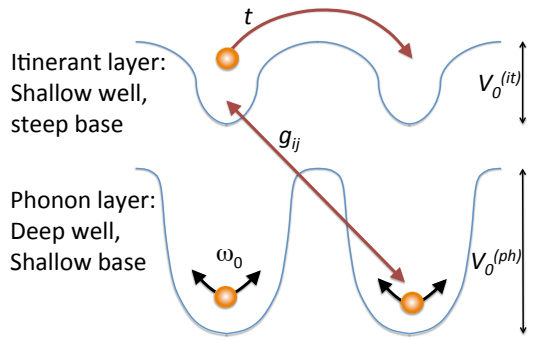

FIG. 1. System of bilayer Rydberg cold atoms for simulation of strong correlations and interactions between fermions and phonons, annotated with Hamiltonian terms. t is the intersite hopping in the itinerant layer, ω_0 the phonon frequency, g_{ij} the Rydberg-phonon coupling and $V_0^{(ph)}$ and $V_0^{(it)}$ are trap depths in the itinerant and phonon layers respectively.

tunable for all interesting physical regimes.

Several schemes for quantum simulation of interactions between electrons and phonons have been suggested. A proposal to bathe bosonic or fermionic impurities in an optical lattice in a BEC [20–22] has led to the observation of polaron effects for bosonic impurities [23]. This succeeds in criterion (1) as the scheme can in principle treat very low fermion density. However, it is essential that Fermionic impurities have a negligible effect on the underlying BEC (specifically, fluctuations in the BEC order parameter must be small [20–22]). This limits the schemes to very low fermion density, voiding criterion (2).

Alternate schemes are based on the interaction between phonons and bosonic excitations. Interactions with high-energy phonon states of Rydberg ions are used as part of the mapping in proposed simulators for spin systems [24, 25]. Li and Lesanovsky have discussed structural distortions associated with exciting high energy Rydberg states in cold ion crystals [26]. Rydberg atoms have been proposed as a way of simulating polaron effects in strongly deformable materials [27]. The use of cold polar molecules to obtain Holstein polaron effects has been discussed [28]. These schemes are not extensible to fermions, so do not fulfil criterion (1), although they are highly tunable. The scheme proposed in this letter goes beyond these as it is capable of simulating interacting Fermions with arbitrary filling factor, while retaining a high level of control over all parameters in the Hamiltonian, thus satisfying all of critera (1), (2) and (3) necessary to examine the complex phase diagrams of strongly correlated systems in the presence of phonons.

We begin by discussing how electron-phonon interactions can be simulated in a system of cold, highly excited (Rydberg) atoms in a bilayer lattice. Over long-ranges, we assume that the Rydberg atoms interact only via dipole-dipole interactions in the strong-coupling Förster regime, $V_{kl} = \mu^2/|\boldsymbol{R}_k - \boldsymbol{R}_l|^3$, where μ is the dipole moment on the Rydberg atom and $\boldsymbol{R}_k$ is the vector to the kth atom in the lattice (see supplementary material for a discussion of the origins of this interaction). The dipole moment may be written in terms of the coefficient C_3 as $\mu = \sqrt{2}C_3$, and depends upon the Rydberg states chosen for the experiment. The ground state atoms have no long range interaction. By coupling the ground $|g\rangle$ and Rydberg $|r\rangle$ states with a laser tuned Δ from the $|g\rangle \rightarrow |r\rangle$ transition and with coupling strength Ω (the Rabi frequency) we mix the states $|g\rangle$ and $|r\rangle$. This technique [29] of dressing the atoms with the laser means that the trapped, ground state atoms acquire the characteristics of the Rydberg state, but in a controllable fashion. In particular, the coefficient C_3 is replaced by an effective interaction coefficient which we write as $C_3' = (\Omega/2\Delta)C_3$. We note that use of a different regime of dipole-dipole interactions has been proposed for the simulation of liquid crystalline phases [30].

The Rydberg atoms, must now be confined in a bilayer lattice. The "itinerant" layer represents the electrons in a condensed matter problem, and the "phonon" layer generates phonon mediated interactions. The itinerant layer can have any filling, and tunneling between adjacent sites is allowed. It is important that the phonon layer has 1 atom per site and that the tunneling is forbidden - the Mott insulator phase [3]. This is achieved by making the potential barrier in the itinerant layer smaller than in the phonon layer. A further complication arises because the atoms in the phonon layer must be set with low oscillating frequencies, while the itinerant layer must be set up with high phonon frequencies. This can be achieved if the optical lattice in the phonon layer has a special configuration as seen in Fig. 1. This form may be achieved using painted potentials [31].

In the itinerant layer, fermions hop with amplitude t, and experience a local Hubbard U, which originates from scattering from the hard-core potential between the fermions when they share the same lattice site [2]. The Hamitonian for these interactions is $H_{\rm Hub} = -t\sum_{\langle i,i'\rangle} c_i^\dagger c_j + U\sum_i n_i n_i$ (n_i is the number operator for fermions on site i, and $c_i^\dagger$ creates a Rydberg atom on site i). Lattice vibrations are introduced by displacing the atoms in the phonon layer. Atomic displacements do not affect the optical lattice, so the vibrations of the atoms are momentum independent Einstein phonons with Hamiltonian, $H_{\rm ph} = \sum_\nu \hbar\omega_{\boldsymbol{k}\nu}(d_{\nu\boldsymbol{k}}^\dagger d_{\nu\boldsymbol{k}} + 1/2)$ and with polarization vectors $\boldsymbol{\xi}_{\boldsymbol{k}\nu} = \boldsymbol{\xi}_\nu$ in orthogonal directions. Here $\omega_{\boldsymbol{k},\nu} = \omega_\nu$ is the angular frequency of a phonon in mode ν with momentum $\boldsymbol{k}$ and $d^\dagger$ and d create and annihilate phonons.

Small in-plane phonon displacements, $\boldsymbol{u}_i$, cause the

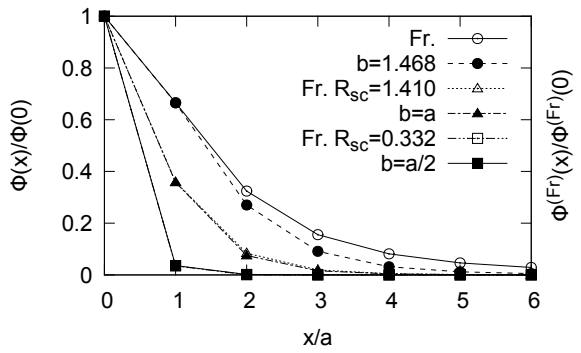

FIG. 2. Comparison between effective Rydberg-Rydberg interactions in the quantum simulator, $\Phi(x)/\Phi(0)$, mediated via phonons in the Rydberg atom system here, and the effective electron-electron interaction, $\Phi^{(\mathrm{Fr})}(x)/\Phi^{(\mathrm{Fr})}(0)$, mediated by phonons in a typical condensed matter system with Fröhlich interactions for various interplane distances. An good correspondence between the effective interactions is seen.

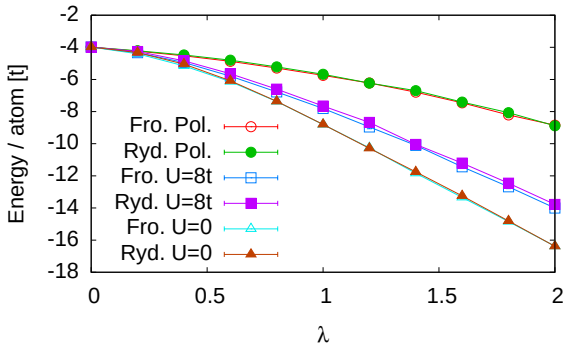

FIG. 3. Comparison of polaron and bipolaron energies calculated for the Rydberg quantum simulator (with $b = 1.468a$), and for a screened Fröhlich interaction in the condensed matter analogue. $\lambda = \Phi(0)/2ztM\omega^2$ and z is the in-plane coordination number. To highlight effects of changes in U, values of 0 and $8t$ are used. The small differences in the tails of the interaction do not strongly affect the physics. $k_BT = 0.014t$, $\omega = 0.2t$. Error bars are smaller than the points.

interaction between Rydberg states to become $V'_{kl} = -\Omega^2\mu^2/4\Delta^2|\boldsymbol{R}_k + \boldsymbol{u}_k - \boldsymbol{R}_l - \boldsymbol{u}_l|^3$, which expands as,

$$V'(\boldsymbol{R}+\boldsymbol{u}) \approx \frac{\Omega^2\mu^2}{4\Delta^2|\boldsymbol{R}|^3} - \frac{3\Omega^2\mu^2\boldsymbol{u}\cdot\hat{\boldsymbol{R}}}{4\Delta^2|\boldsymbol{R}|^4}. \tag{1}$$

The phonons are quantized by substituting $\boldsymbol{u}_i = \sum_{\boldsymbol{k},\nu}\sqrt{\hbar/2NM\omega_{\boldsymbol{k},\nu}}\boldsymbol{\xi}_{\boldsymbol{k},\nu}(d_{\boldsymbol{k},\nu}e^{-i\boldsymbol{k}\cdot\boldsymbol{R}_i} + d^\dagger_{\boldsymbol{k},\nu}e^{i\boldsymbol{k}\cdot\boldsymbol{R}_i})$. Since all sites in the phonon layer are occupied, and the modes momentum independent, a multimode Rydberg-phonon interaction with extended Holstein form is derived,

$$H_{\mathrm{R-ph}} = \frac{3\mu^2\Omega^2}{4\Delta^2}\left(\frac{\hbar}{2M\omega_0}\right)^{1/2}\sum_\nu\sum_{ij}\frac{\hat{\boldsymbol{R}}_{ij}\cdot\boldsymbol{\xi}_\nu}{R^4_{ij}}n_i(d^\dagger_{j,\nu}+d_{j,\nu}) \tag{2}$$

Here, $\boldsymbol{R}_{ij}$ is a vector between an atom in the itinerant layer at site i, and an atom in the phonon layer at site j, N the number of sites and M is the mass of the atoms. The presence of multiple phonon modes in the Hamiltonian is interesting since such interactions are difficult to simulate with current numerical techniques.

A further simplification can be made by elongating the potentials in the phonon layer along the direction perpendicular to the planes, so that the Hamiltonian becomes, $H_{\mathrm{Holstein}} = \sum_{ij} g_{ij}n_i(d^\dagger_j + d_j)$ with the interaction, $g_{ij} = \frac{\Omega^2}{4\Delta^2}\frac{3\mu^2 b}{(b^2+r^2_{ij})^{5/2}}\left(\frac{\hbar}{2M\omega_0}\right)^{1/2}$. where r_{ij} is the distance between the projection of sites i and j onto the same layer and b is the interplane distance. To compare with condensed matter analogues, a Holstein model, where the local electron density couples to local optical phonon modes [18], has $g^{(\mathrm{Hol})}_{ij} \sim \delta_{ij}$. In other condensed matter systems, Fröhlich electron-phonon interaction generalized to lattice models (also known as the extended Holstein interaction) has the form $g^{(\mathrm{Fr})}_{ij} \sim \exp(-r_{ij}/R_{sc})(b^2+r^2_{ij})^{-3/2}$ where R_{sc} is a screening radius[32].

When the phonon energy is much larger than hopping, the effective instantaneous interaction between Rydberg atoms in the itinerant layer mediated though the phonon layer is $-zt\lambda\sum_{\boldsymbol{m}}\Phi(\boldsymbol{r})/\Phi(0)$ where $\Phi(\boldsymbol{r})/\Phi(0) = \sum_{\boldsymbol{m}} g_{\boldsymbol{r},\boldsymbol{m}}g_{0,\boldsymbol{m}}/\sum_{\boldsymbol{m}} g_{0,\boldsymbol{m}}g_{0,\boldsymbol{m}}$. Fig. 2 shows a comparison between the shapes of Rydberg and lattice Fröhlich effective interactions $\Phi^{(\mathrm{Fr})}(x)/\Phi^{(\mathrm{Fr})}(0)$ for various interplane distances and screening radii (a is the intersite distance in the plane). As would be done in the experiment, the near-neighbor interactions are matched by modifying b to get the closest possible correspondence to the Fröhlich interaction that is to be simulated. An excellent correspondence between the shapes of the interactions is seen for interplane distance $b \lesssim a$. The origin of the effective interaction is discussed in the supplement.

To demonstrate the scheme, we use CTQMC [33] to compute the properties of polarons and bipolarons in the bilayer lattice and compare with results from the screened Fröhlich interaction (Fig. 3). The simulations include phonon-mediated interactions, the Hubbard U, and also the small direct dipole-dipole interaction between atoms in the itinerant layer, $H_{\mathrm{direct}} = \sum_{i\neq i'} V_{ii'}n_in_{i'}$ (as discussed in the supplementary material). A very close agreement is found between the quantum simulator and Fröhlich system, further demonstrating that the small differences in the tails of the interaction and the residual long-range interactions in the itinerant layer do not affect local pairing.

Finally, we discuss a realistic experimental setup for building the quantum simulator. We recommend that experimentalists stage their investigations by using easier to control bosonic Rydberg atoms before moving on to fermions. A bilayer optical lattice may be set up with painted potentials [31], a powerful technique with a high

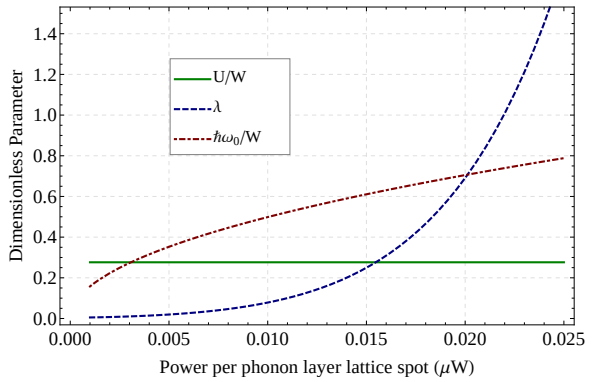

FIG. 4. Dimensionless parameters for rubidium atoms in the proposed spot potential experiment. All physically relevant regimes are accessible by tuning the spot power in the itinerant and phonon layers ($W = zt$). Further control of λ is possible by changing the detuning, Δ.

level of control. Creating a bilayer painted lattice requires two focused horizontal sheets. Gaussian spots of waist $w^{(it)}$ are focussed on the itinerant sheet, and pairs of spots with waist $w^{(ph)}$ separated by a distance $2D$ are painted in the phonon layer. The resulting lattices are filled with Rb atoms and detuned from the 48S state by $\Delta = 125$MHz, with $\Omega = 10$MHz leading to $\mu^2 = 173$MHz (N.B. The values found here for the bosonic Rb are representative of all alkali Rydberg atoms). Fig. 4 shows the dimensionless parameters calculated for a realistic set up, with $a = 2.62\mu$m and $b = 3.67\mu$m. Spot lattices in the itinerant layer have $w^{(it)} = 2.46\mu$m, so the potentials overlap leading to a near sinusoidal potential with $V_0^{(it)} = 70.1$Hz and energy level spacing in the itinerant layer of 153Hz, $U = 5.34$Hz, $t = 4.83$Hz, so a one band model will be simulated. Phonon frequencies are easily changed in the phonon layer by tuning D, and can therefore be changed independently. As an example, with $V_0^{(ph)} = 578$Hz, $w^{(ph)} = 0.655\mu$m and $D = 0.999w^{(ph)}$, $\omega_0^{(ph)} = 13.8$Hz and $\lambda = 1.00$ is achieved - challenging but possible with a state of the art diffraction-limited optical arrangement. A simpler 1D version of the experiment that only requires a single horizontal sheet can be performed using two coupled chains (a phonon chain and an itinerant chain) and is recommended as a starting place when implementing the experiment. In 1D, we find equally good correspondence between the quantum simulator and condensed matter analogue.

In the bilayer system, the interesting physics are encoded in the momentum distribution of the gas held in the itinerant layer. What we want to study is the correlation function $C(\boldsymbol{k}, \sigma; -\boldsymbol{k}, -\sigma)$. To extract this, the momentum distribution must be observable. In the experiments in Ref. 34, this was accomplished using a time-of-flight method, where the momentum distribution of the roaming atoms is mapped onto the spatial location at the time of imaging.

Since it is the purpose of the proposed system to understand phase diagrams, we briefly note the effect that different interaction types have in forming and modifying these phases. Repulsive Hubbard U promotes a Mott insulating state and antiferromagnetism close to half-filling, and may promote superconductivity through spin fluctuations. It may also control the form of the superconductivity, reducing or eliminating s-wave pairing. Direct in-plane V_{ij} may promote charge ordering and suppress superconductivity if it is repulsive, and could enhance superconductivity when attractive. Interaction with phonons promotes BCS superconductivity at weak coupling, and a BEC of bipolarons for large λ.

In this letter, we have shown how systems of cold Rydberg atoms in a bilayer can be used as a simulator for electron-phonon interactions in the presence of strong electronic correlation, of the type found in many unconventional superconductors. We have carried out the mapping to an extended Hubbard–Holstein model and used numerics to demonstrate the simulator is capable of reproducing the pairing and polaron physics of standard electron-phonon models. Furthermore, we have described how the simulator can be implemented using contemporary techniques. The proposed system goes well beyond the possibilities of previous quantum simulators for the simulation of interactions with lattice vibrations. In particular, we can reliably simulate half filled femion systems relevant to cuprate and other unconventional superconductors, tune all parameters directly through the optical lattice and can easily include multiple phonon modes.

JPH acknowledges EPSRC grant EP/H015655/1 and CM grant EP/F031130/1. We thank I. Lesanovsky, M. Bruderer, F. Herrera, A. Kowalczyk, N. Braithwaite, S. Bergamini, S. Alexandrov and J. Samson for useful discussions, and especially thank Pavel Kornilovitch for longstanding collaboration on QMC and polarons.

[1] J. Hubbard. *Proc. R. Soc. A*, 276:238, 1963.
[2] I. Bloch, J. Dalibard, and W. Zwerger. *Rev. Mod. Phys.*, 80:885, 2008.
[3] M. Greiner *et al. Nature*, 415:39, 2002.
[4] G. K. Campbell *et al. Science*, 313:649, 2006.
[5] A. Hebard et al. *Nature*, 350:600, 1991.
[6] T.T.M. Palstra et al. *Solid St. Commun.*, 93:327, 1995.
[7] A.Y. Ganin *et al. Nature*, 466:221, 2010.
[8] R.J. Cava *et al. Nature*, 332:814, 1988.
[9] I.B. Bischofs, V.N. Kostur, and P.B. Allen. *Phys. Rev. B*, 65:115112, 2002.
[10] B. Batlogg *et al. Phys. Rev. Lett.*, 61:1670, 1988.
[11] D.G. Hinks *et al. Nature*, 335:419, 1988.
[12] R.J. Cava et al. *Nature*, 367:146, 1994.
[13] Z. Hossain et al. *Solid St. Commun.*, 92:341, 1994.
[14] H. Kawaji S. Yamanaka, K. Hotehama. *Nature*, 392:580, 1998.

[15] P.W. Anderson. *The Theory of Superconductivity in the Cuprates*. Princeton University, Princeton NY, 1997.

[16] G.M.Zhao et al. *J. Phys.: Condens. Matter*, 13:R569, 2001.

[17] A. Lanzara *et al. Nature*, 412:6846, 2001.

[18] T. Holstein. *Ann. Phys.*, 8:325, 1959.

[19] E. Gull *et al. Rev. Mod. Phys.*, 83:349, 2011.

[20] M. Bruderer, A. Klein, S. R. Clark, and D. Jaksch. *Phys. Rev. A*, 76:011605(R), 2007.

[21] M. Bruderer *et al. Phys. Rev. A*, 82:043617, 2010.

[22] A. Privitera and W. Hofstetter. *Phys. Rev. A*, 82:063614, 2010.

[23] B. Gadway, D. Pertot, R. Reimann, and D. Schneble. *Phys. Rev. Lett.*, 105:045303, 2010.

[24] D. Porras and J. I. Cirac. *Phys. Rev. Lett.*, 92:207901, 2004.

[25] M. Müller, L. Liang, I. Lesanovsky, and P. Zoller. *New J. Phys.*, 10:093009, 2008.

[26] W. Li and I. Lesanovsky. *Phys. Rev. Lett.*, 108:023003, 2012.

[27] J.P. Hague and C. MacCormick. *New J. Phys.*, 14:033019, 2012.

[28] F. Herrera and R. V. Krems. *Phys. Rev. A*, 84:051401, 2011.

[29] N. Henkel, R. Nath, and T. Pohl. *Phys. Rev. Lett.*, 104:195302, 2010.

[30] J. Quintanilla, S.T. Carr, and J.J. Betouras. *Phys. Rev. A*, 79:031601(R), 2009.

[31] K. Henderson, C. Ryu, C. MacCormick, and M.G. Boshier. *New J. Phys.*, 11:043030, 2009.

[32] A.S. Alexandrov and P.E. Kornilovitch. *Phys. Rev. Lett.*, 82:807, 1999.

[33] J.P. Hague and P.E. Kornilovitch. *Phys. Rev. B*, 80:054301, 2009.

[34] W. S. Bakr *et al. Science*, 329:547, 2010.

Supplementary Material: Bilayers of Rydberg atoms as a quantum simulator for unconventional superconductors.

ORIGIN OF DIPOLE-DIPOLE INTERACTIONS BETWEEN RYDBERG ATOMS

We present the simplest formulation necessary for studying the dipole-dipole interaction between two Rydberg atoms which we take to be excited to the $|nS_{1/2}\rangle$ state, seperated by a distance R. First, we write down the dipole-dipole Hamiltonian:

$$V_{\mathrm{dip-dip}} = \frac{1}{4\pi\epsilon_0}\left(\frac{\boldsymbol{\mu_1}\cdot\boldsymbol{\mu_2}}{R^3} - \frac{3\left(\boldsymbol{\mu}_1\cdot\boldsymbol{R}\right)\left(\boldsymbol{\mu}_2\cdot\boldsymbol{R}\right)}{R^5}\right) \quad (1)$$

where the dipole moments $\boldsymbol{\mu}_i$ are given as $\boldsymbol{\mu}_i = e\boldsymbol{r}_i$, e being the electron charge and $\boldsymbol{r}_i$ the position operator for atom i. $V_{\mathrm{dip-dip}}$ couples our initial pair state $|nS_{1/2}; nS_{1/2}\rangle$ to other pair states, but we need only consider pair states with similar enrgy to our initial state. For simplicity, we specialize to the case where one other pair-state dominates the interaction: $|n'P_{j'}; n''P_{j''}\rangle$. Generalising to a more realistic situation is possible, see for example [1].

$$V_{\mathrm{Int}} = \begin{pmatrix} 0 & V(R) \\ V(R) & \Delta_{sp} \end{pmatrix} \quad (2)$$

where $V(R) = \langle nS_{1/2}; nS_{1/2}|V_{\mathrm{dip-dip}}|n'P_{j'}; n''P_{j''}\rangle$ and $\Delta_{sp} = 2E(nS_{1/2}) - E(n'P_{j'}) - E(n''P_{j''})$ is the difference in energy of the two states, with $E(nL_j)$ being the energy of a single isolated atom in the state nL_j. As a consequence of the average over states, there is no preferred direction to $V(R)$.

Diagonalising this Hamiltonian yields the interaction energy eigenvalues: $V_{\mathrm{Int}\pm} = \Delta_{sp}/2 \pm \sqrt{4V(R)^2 + \Delta_{sp}^2}/2$. Two extreme regimes exist, found by expanding $V_{\mathrm{Int}\pm}$ appropriately. In the van der Waals regime, $V(R) \ll \Delta_{sp}$ such that the mixing of the two basis states is small and the $|nS_{1/2}; nS_{1/2}\rangle$ state corresponds to the eigenstate with $V_{\mathrm{Int}-}$ which is shifted by $\delta V(R) \approx -V(R)^2/\Delta_{sp}$, so the energy scales as $1/R^6$ (see eq.(1)). In this case, we define the C_6 coefficient by setting $\delta V(R) = -C_6/R^6$. In the dipole-dipole regime, $V(R)$ dominates Δ_{sp} and the two pair states are mixed appreciably. In this case the eigenstates of the Hamiltonian are shifted by $\delta V(R) \approx \pm V(R)$ these energies scaling as $1/R^3$ (by changing the energy of the laser, it is possible to select either the attractive or repulsive form of $\delta V(R)$). We define the C_3 coefficient by setting $\delta V(R) \approx V(R) = \pm C_3/R^3$. The latter regime is appropriate in this paper because C_3 is large enough, and the distance small enough that the interaction is dominated by its C_3/R^3 character.

Finally, we note that sometimes there are couplings between the $nS_{1/2}$ states (which themselves are spherically symmetric), and several nearby nP_j. Numerical treatments show that in this case the interaction acquires a slight angular dependency which differs from spherical symmetry by less than 5%, and angular dependence can be safely neglected.

PROPERTIES OF PAINTED SPOT POTENTIALS

We make the itinerant layer from large overlapping Gaussian spots in an optical pancake, which forms a sinusoidal pattern similar to a conventional optical lattice. Since the form of the potential in that layer is almost sinusoidal, the parameters of the itinerant layer can be read from Bloch *et al.* [2]:

$$t^{(it)} \approx \frac{4}{\sqrt{\pi}} E_{\mathrm{rec}} \left(\frac{V_0}{E_{\mathrm{rec}}}\right)^{3/4} \exp\left[-2\left(\frac{V_0}{E_{\mathrm{rec}}}\right)^{1/2}\right] \quad (3)$$

where V_0 is the difference between the maximum and minimum values of the periodic potential. $E_{\mathrm{rec}} = \hbar^2k^2/2M$ is the recoil energy of the lattice, M the atomic mass and $k = \pi/a$ with a the lattice constant. In this layer, we also have that:

$$U^{(it)} \approx \sqrt{\frac{8}{\pi}} k\tilde{a} E_{\mathrm{rec}} \left(\frac{V_0}{E_{\mathrm{rec}}}\right)^{3/4}. \quad (4)$$

where $\tilde{a}$ is the s-wave scattering length. It is also worth checking that Harmonic oscillations are not excited in the itinerant layer, which has phonon frequency,

$$\hbar\omega_0^{(it)} = 2E_{\mathrm{rec}} \left(\frac{V_0}{E_{\mathrm{rec}}}\right)^{1/2} \quad (5)$$

Essentially, the distance between oscillator levels is the energy difference between fermion bands when the value is very large.

In the phonon layer, we require that the potential is deep so that hopping is weak and Hubbard U is large (which also acts against hopping). However, we require that phonon frequency is also low. To achieve this, pairs of spots create a potential with the form,

$$-\frac{V_0^{(ph)}}{2}\left[\exp\left(-\frac{(x-D)^2}{2w^{(ph)^2}}\right) + \exp\left(-\frac{(x+D)^2}{2w^{(ph)^2}}\right)\right] \quad (6)$$

(where the depth of the potential in the phonon layer is $V_0^{(ph)}$). The Taylor expansion leads to the phonon frequency,

$$(\omega_0^{(ph)})^2 = V_0^{(ph)} \exp\left(-D^2/2w^{(ph)^2}\right) \frac{(w^{(ph)^2} - D^2)}{Mw^{(ph)^4}}. \quad (7)$$

We only need order of magnitude estimates for $t^{(ph)}$ and $U^{(ph)}$. We use the lowest order harmonic of the lattice and the same equations as for the itinerant layer to calculate $t^{(ph)}$. For $U^{(ph)}$, the same equation is used, but with a modified confinement length.

Finally it is necessary to calculate the dimensionless electron-phonon coupling, which has the form:

$$\lambda = \frac{1}{2\omega_0^2 MW}\left[\frac{3\Omega^2\mu^2}{4\Delta^2}\right]^2 \sum_i \frac{b^2}{(b^2+r_{0i}^2)^5} \tag{8}$$

where $W = 4t^{(it)}$ is the half-band width.

RYDBERG-PHONON INTERACTION AND THE EFFECTIVE RYDBERG-RYDBERG INTERACTION MEDIATED VIA PHONONS

In this section we provide a brief overview explaining how an effective Rydberg-Rydberg interaction between atoms in the itinerant layer can be mediated through atoms in the phonon layer. We will look at the interactions when the phonon frequency is very large, where we can use the Lang-firsov transformation to derive the effective interaction. We will also demonstrate the same transformation using the Fröhlich interaction between electrons in a plane and phonons in a neighbouring plane. For moderate and small phonon frequencies, the interaction has the same spatial form, but is also retarded. The form of the action used to simulate small phonon frequencies can be found in Ref. [3] and references therein.

We will concentrate on the phonon and interaction terms in the Hamiltonian. The Lang-firsov transformation has the form:

$$\tilde{H} = e^{-S} H e^{S} \tag{9}$$

where $S = \sum_{ij} g_{ij} n_i (d_j^\dagger - d_j)/\hbar\omega_0$. After some algebra, transformed Rydberg atom creation operators and phonon creation operators are found,

$$\tilde{c}_i^\dagger = c_i^\dagger \exp\left[\sum_j g_{ij}\left(d_j^\dagger - d_j\right)/\hbar\omega_0\right] \tag{10}$$

$$\tilde{d}_j^\dagger = d_j^\dagger + \sum_i g_{ij} n_i/\hbar\omega_0. \tag{11}$$

By substitution into $H_{\rm ph} + H_{\rm R-ph}$, a transformed Hamiltonian is found.

$$\tilde{H}_{int} = -W\lambda \sum_{ii'} n_i n_{i'} \frac{\Phi_{i'-i}}{\Phi_0} + \hbar\omega_0 \sum_j \left(d_j^\dagger d_j + \frac{1}{2}\right), \tag{12}$$

In this Hamiltonian, Rydberg and electron terms are separated, and an phonon mediated effective Rydberg-Rydberg interaction in the itinerant plane is derived. Here,

$$\Phi_i = \sum_j g_{j0} g_{ji} \tag{13}$$

For the interaction in this article,

$$g_{ij} = \frac{\Omega^2}{4\Delta^2}\frac{3\mu^2 b}{(b^2+r_{ij}^2)^{5/2}}\left(\frac{\hbar}{2M\omega_0}\right)^{1/2} \tag{14}$$

and,

$$\lambda = \frac{\sum_j g_{0j}^2}{\hbar\omega_0 W} = \frac{\Phi_0}{\hbar\omega_0 W}. \tag{15}$$

It is interesting to note that it doesn't matter if g is attractive or repulsive, the effective interaction is always attractive. This can be understood in the following way. An attractive interaction pulls atoms in the phonon layer towards itinerant Rydberg atoms. A subsequent Rydberg atom will have a lower energy if the atom in the phonon layer is closer to the itinerant layer. thus, an attractive interaction is formed.

Alternatively, a repulsive interaction pushes atoms in the phonon layer away from atoms in the itinerant layer. A subsequent Rydberg atom will have a lower energy if the atom in the phonon layer is further from the itinerant layer, and so will be attracted to the location where the first atom was. Therefore, a repulsive inter-layer interaction also leads to an effective attraction. The only circumstance under which g can generate an effective repulsive interaction is if the sign of g changes somewhere in space.

FRÖHLICH ELECTRON-PHONON INTERACTION AND THE EFFECTIVE ELECTRON-ELECTRON INTERACTION IN CONDENSED MATTER ANALOGUES

The Fröhlich interaction can be found in quasi 2D layered materials where electrons or holes are confined to 2D planes and couple with phonons in a neighboring plane. For such a system, the argument above also applies, but now we use the operator $c_{\rm el}^\dagger$ to create electrons rather than Rydberg atoms. The interaction between electrons and phonons in a different plane $g_{ij}^{(\rm Fr)} \sim \exp(-r_{ij}/R_{sc})(b^2+r_{ij}^2)^{-3/2}$ where R_{sc} is a screening radius [4]. There are quantitative differences between the effective phonon mediated interaction Φ for the Rydberg cold atom simulator and the effective interaction $\Phi_{\rm Fr}$ the condensed matter analogue with Fröhlich interaction, but the qualitative shape and attractive nature of the effective interactions are the same.

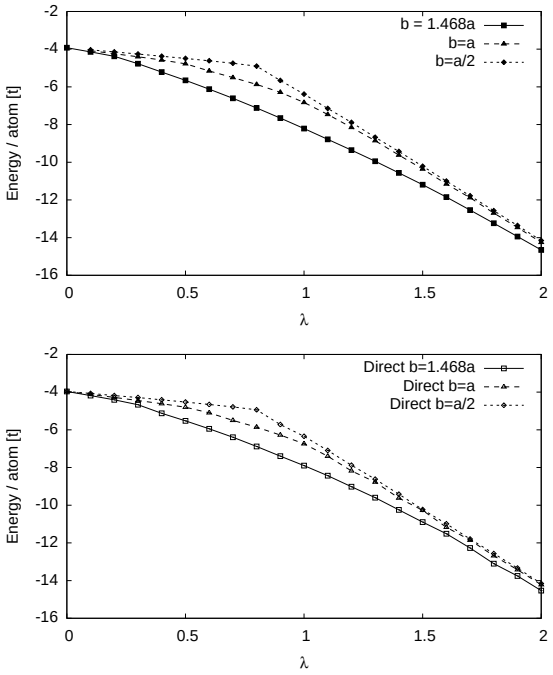

FIG. 1. Comparison between bipolaron energy for the quantum simulator system including (bottom) and neglecting (top) direct in plane interactions, using the parameters in the text. There are only small differences between the energies, with the differences decreasing with the distance between planes (or chains in the 1D case).

DIRECT RYDBERG-RYDBERG INTERACTION IN THE PLANE

The remaining interaction to be considered is the direct interaction between Rydberg atoms in the itinerant layer. Using the definitions of λ and g_{ij}, it is possible to rewrite the tunable parameter $3\mu^2\Omega^2/4\Delta^2$ in terms of λ so that the direct in-plane interaction $V_{ij} = \Omega^2\mu^2/4\Delta^2 r_{ij}^3$ can be established. Thus,

$$V_{ij} = \frac{\left(2M\omega_0^2\lambda W\right)^{1/2}}{3r_{ij}^3}\left[\sum_k \frac{b^2}{(b^2+r_{0k}^2)^5}\right]^{-1/2} \tag{16}$$

Since this interaction depends on $\sqrt{\lambda}$, it will be negligible compared to the effective Rydberg-Rydberg interaction mediated by the phonon layer for sufficiently large λ. The coefficient $\chi = \frac{\left(2M\omega_0^2\lambda W\right)^{1/2}}{3r_{ij}^3}\left[\sum_k \frac{b^2}{(b^2+r_{0k}^2)^5}\right]^{-1/2}\frac{\Phi_0}{t\lambda\Phi_{i-j}}$ gives the relative strength of the interactions. For rubidium with the parameters $b = a$, $M = 1.45\times10^{-25}$kg, $\omega_0 \sim t/\hbar \sim 10$Hz, $r_{ij} \sim 1\mu$m, and $\Phi_1 \sim 1/3$, it is found that $\chi \sim 0.3/\sqrt{\lambda}$, which means that intersite terms achieve similar magnitude only below $\lambda \sim 0.1$. It may initially seem curious that the 2nd order effect of effective Rydberg-Rydberg interaction is stronger under certain conditions. This can be explained because (a) the effective interaction involves many pairs of atoms, whereas the direct interaction only involves a single pair. (b) The effective Rydberg-Rydberg interaction is retarded, so atoms may remain far apart spatially while locally interacting strongly. Point (b) is manifest because there is a prefactor of ω_0 when the direct interaction is rewritten in terms of $\sqrt{\lambda}$. So as phonon frequency increases and the effective interaction becomes more instantaneous, the direct interaction dominates. For realistic low phonon frequencies where retardation effects are very strong and interactions act over long periods of time, the effective interaction dominates, a view backed up by the numerics shown in the figure.

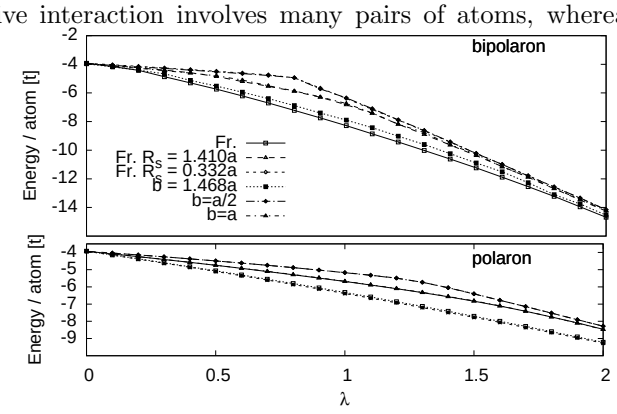

FIG. 2. Polaron and bipolaron energies for a range of interplane spacings, b and corresponding Fröhlich screening R_{sc}.

INTER-PLANE SPACING

For comparison, the bipolaron and polaron energies are calculated for a range of interplane spacings b and correponding Fröhlich screening R_{sc} (Fig. 2). As the interplane spacings become smaller and the interaction approaches the Holstein interaction, the two schemes converge. Here $\omega = t$, $\beta = 1/k_BT = 14/t$. At the higher phonon frequencies used here (compared to the main text) there is a small difference between the energies of the quantum simulator and the Fröhlich interaction due to the small residual direct in-plane interaction, which vanishes as the phonon frequency decreases.

A BRIEF OVERVIEW OF THE QMC ALGORITHM

We briefly summarise the continuous time QMC algorithm for bipolarons used for numerical aspects of this paper. Full details of our algorithm can be found in Refs. 5 and 6. The algorithm is a path integral variant of continuous time QMC. After integrating out the phonons, the action is,

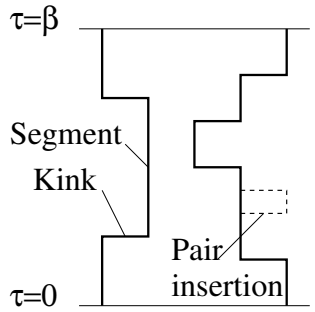

FIG. 3. Schematic of paths for the continuous time quantum Monte Carlo algorithm used to obtain numerical results. The dashed lines show insertion of a kink-antikink pair to a single path.

$$A[\{\boldsymbol{r}\}] = \frac{z\lambda\bar{\omega}}{2\Phi_0(0,0)} \int_0^{\bar{\beta}} \int_0^{\bar{\beta}} d\tau d\tau' e^{\frac{-\bar{\omega}\bar{\beta}}{2}} \sum_{ij} \Phi_0[\boldsymbol{r}_i(\tau), \boldsymbol{r}_j(\tau')](e^{\bar{\omega}(\frac{\bar{\beta}}{2}-|\tau-\tau'|)} + e^{-\bar{\omega}(\frac{\bar{\beta}}{2}-|\tau-\tau'|)}) - \frac{1}{2}\sum_{i\neq j}\int_0^{\beta} v(\boldsymbol{r}_i(\tau), \boldsymbol{r}_j(\tau))d\tau,$$

where $\bar{\beta} = \beta t$, $\bar{\omega} = \omega/t$ and v is the direct instantaneous interaction. N.B. the action is slightly simplified compared to the references because we do not calculate the inverse mass, so periodic boundary conditions in time are used. In spite of the integration over phonons, it is still more expensive to simulate the electron-phonon problem at low phonon frequencies because of retardation effects (which show up in the double integral between the paths at different imaginary times).

Paths consist of segments and kinks (Fig. 3). The algorithm proceeds by adding or removing pairs of kinks and antikinks (an antikink is a kink in the opposite direction) according to the probability,

$$P(\text{addition}) = \min\left\{1, t^2\beta e^{A(D)-A(C)}/N_{\boldsymbol{l}A}(D)N_{-\boldsymbol{l}A(D)}\right\} \tag{17}$$

$$P(\text{removal}) = \min\left\{1, N_{\boldsymbol{l}A}(D)N_{-\boldsymbol{l}A(D)}/t^2\beta e^{A(D)-A(C)}\right\} \tag{18}$$

with both kinks inserted relative to the top or bottom of the path (here D represents the paths with 2 additional kinks than path configuration C). In an exchanged configuration of paths a slightly different update can be used, inserting a kink on one path, and an anti-kink on the other:

$$P(\text{addition}) = \min\left\{1, t^2\beta e^{A(D)-A(C)}/N_{\boldsymbol{l}A}(D)N_{-\boldsymbol{l}B(D)}\right\} \tag{19}$$

$$P(\text{removal}) = \min\left\{1, N_{\boldsymbol{l}A}(D)N_{-\boldsymbol{l}B(D)}/t^2\beta e^{A(D)-A(C)}\right\}. \tag{20}$$

Details on the subtleties of exchange can be found in Ref. 5. Efficiency can be improved by exchanging path ends by inserting multiple kinks (see Ref. 5). Details of extension to 2D can be found in Ref. 6. If the ends of both paths lie on the same site, both sets of updates can be used.

Averages of physical properties are taken every few Monte Carlo steps. The appropriate estimator for the energy is,

$$E = -\lim_{\beta\to\infty}\left[\left\langle\frac{\partial A}{\partial\beta}\right\rangle + \frac{1}{\beta}\left\langle\sum_i N_i\right\rangle\right]. \tag{21}$$

Error bars are calculated using a bootstrap method.

[1] T. G. Walker and M. Saffman, Phys. Rev. A **77**, 032723 (2008).
[2] I. Bloch, J. Dalibard, and W. Zwerger, Rev. Mod. Phys. **80**, 885 (2008).
[3] J.P.Hague, P.E.Kornilovitch, J.H.Samson, and A.S.Alexandrov, J. Phys.: Condens. Matter **19**, 255214 (2007).
[4] A. Alexandrov and P. Kornilovitch, Phys. Rev. Lett. **82**, 807 (1999).
[5] J. Hague and P. Kornilovitch, Phys. Rev. B **80**, 054301 (2009).
[6] J. Hague and P. Kornilovitch, Phys. Rev. B **82**, 094301 (2009).